

Chapter 10. The Collapse of Dense Cores

Notes:

- *Most of the material presented in this chapter is taken from Stahler and Palla (2004), Chap. 10.*

10.1 Ambipolar Diffusion

In Chapter 9 we have successively studied cases where magnetic fields were either not considered or included in models of isothermal clouds equilibrium and stability. We now refine our model by considering the **ambipolar diffusion** phenomenon, which happens when the neutral component of the gas ceases to be perfectly coupled to the ionized component (i.e., electrons and ions). Since the ionized gas is coupled to the magnetic field lines, it follows that the neutrals are slipping by the field lines when ambipolar diffusion is occurring. That is, as far as the neutrals are concerned the magnetic flux is *diffusing* away from the main component of the gas, hence the name.

We start with the evaluation of the **drift velocity** of the ions (or electrons, since they are moving with a similar, but not exactly the same, mean velocity)

$$\mathbf{v}_d \equiv \mathbf{u}_i - \mathbf{u}, \quad (10.1)$$

where \mathbf{u}_i and \mathbf{u} are the ion and neutral mean velocity, respectively. We know from the solution for Problem 5 of the First Assignment that the equations of motion for the ions and electrons can be combined (neglecting the inertial terms) to give

$$\mathbf{v}_d n_i (\mu_i \nu_i + \mu_e \nu_e) = \frac{1}{c} \mathbf{j} \times \mathbf{B}, \quad (10.2)$$

where n_i is the volume density of ions (and electrons, from global charge neutrality considerations), and the pairs of μ and ν stand for the reduced mass and collision rates for the ions and electrons resulting from their collisions with the neutral particles. Using Ampère's law we transform equation (10.2) to

$$\begin{aligned} \mathbf{v}_d &= \frac{(\nabla \times \mathbf{B}) \times \mathbf{B}}{4\pi n_i (\mu_i \nu_i + \mu_e \nu_e)} \\ &\simeq \frac{(\nabla \times \mathbf{B}) \times \mathbf{B}}{4\pi n_i \mu_i \nu_i}, \end{aligned} \quad (10.3)$$

since $\mu_i \gg \mu_e$. The collision rate of a charge with neutral particles is a constant at low-enough drift speed with (see equation (5.9) of the Lecture Notes)

$$\nu_i \simeq 10^{-9} n \text{ s}^{-1}, \text{ when } |\mathbf{v}_d| \lesssim 10 \text{ km s}^{-1}. \quad (10.4)$$

If we consider once again the equation of motion for the ions, while neglecting the inertial term and assuming that the Lorentz force dictates their motion (i.e., the ions are tied to the magnetic field), then we simply have for Ohm's law

$$\begin{aligned}\mathbf{E} &\simeq -\frac{\mathbf{u}_i}{c} \times \mathbf{B} \\ &= -\frac{1}{c}(\mathbf{v}_d + \mathbf{u}) \times \mathbf{B},\end{aligned}\tag{10.5}$$

which we insert into Faraday's law of induction to get

$$\begin{aligned}\frac{\partial \mathbf{B}}{\partial t} &= -c(\nabla \times \mathbf{E}) \\ &\simeq \nabla \times (\mathbf{u} \times \mathbf{B}) + \nabla \times (\mathbf{v}_d \times \mathbf{B}).\end{aligned}\tag{10.6}$$

The first term on the right hand side of equation (10.6) is the so-called convective term that is responsible for flux freezing, while the last term is a non-linear function of the magnetic field (from equation (10.3)) and is the diffusive term that leads to the diffusion of the magnetic field lines. Our story is therefore consistent, as the existence of a drift velocity (which implies ambipolar diffusion) cause the diffusion of the magnetic field. The ratio of the convective to the diffusive terms of equation (10.6) yields the so-called **magnetic Reynolds number**

$$\begin{aligned}R_m &= \frac{\nabla \times (\mathbf{u} \times \mathbf{B})}{\nabla \times (\mathbf{v}_d \times \mathbf{B})} \\ &\simeq \frac{4\pi n_i \mu_i v_i L V}{B^2},\end{aligned}\tag{10.7}$$

where L and V ($\approx u \approx v_d$) are characteristic length and speed for our analysis. When conditions are such that $R_m \gtrsim 1$ then flux freezing prevails. On the other hand, ambipolar diffusion becomes important when $R_m \lesssim 1$. The relevant time scale for ambipolar diffusion, $L/|\mathbf{v}_d|$, can be evaluated directly from equation (10.3) or with equation (10.7) (when setting $V \approx |\mathbf{v}_d|$ and $R_m \approx 1$)

$$\begin{aligned}\frac{L}{|\mathbf{v}_d|} &\simeq \frac{4\pi n_i \mu_i v_i L^2}{B^2} \\ &\simeq 3 \times 10^6 \left(\frac{n_{\text{H}_2}}{10^4 \text{ cm}^{-3}} \right)^{3/2} \left(\frac{B}{30 \mu\text{G}} \right)^{-2} \left(\frac{L}{0.1 \text{ pc}} \right)^2 \text{ yr},\end{aligned}\tag{10.8}$$

where we used $n_i = n_e \approx 1 \times 10^{-5} n_{\text{H}_2}^{-1/2}$ (see equation (8.46) of the Lecture Notes). We therefore see that this time scale is relevant for dense cores, as it compares well to their observed life times.

10.1.1 Magnetic Flux Loss

In the magnetic model of Chapter 9 we determined the variation in mass relative to that of the magnetic flux ratio $dM/d\Phi_B$ (see equation (9.54)) and assumed it to hold at all times because of flux freezing. We now see, however, that this assumption needs to be corrected for the presence of ambipolar diffusion.

The temporal change in mass with a surface containing a fixed amount of magnetic flux is given by

$$\left(\frac{\partial M}{\partial t}\right)_{\Phi_B} = \int_S \rho \mathbf{v}_d \cdot \mathbf{n} da, \quad (10.9)$$

where \mathbf{n} is the unit vector normal to the surface S , and the Φ_B subscript implies that the corresponding quantity is evaluated on the surface containing the magnetic flux.. The first thing to realize is that the drift velocity is directed perpendicular to \mathbf{B} (from equation (10.3)) and therefore to the surface (i.e., it is parallel to \mathbf{n}). Equations (9.42) of the previous chapter also tells us that

$$\frac{1}{c} \mathbf{j} \times \mathbf{B} = e^{-\Phi_B/a_T^2} \nabla q, \quad (10.10)$$

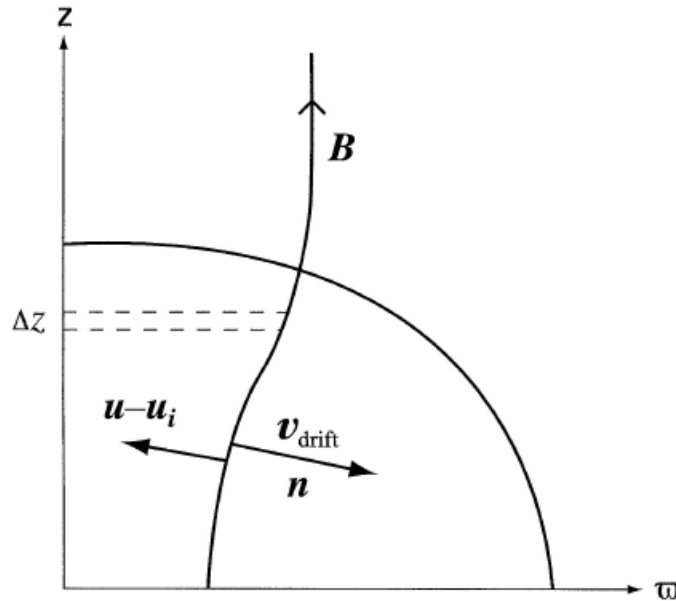


Figure 10.1 – Illustration of ambipolar diffusion in a magnetized core. The drift velocity is in a direction perpendicular to the surface containing the magnetic flux.

which when combined with Ampère's law and equation (10.2) gives (with $\mu_i \gg \mu_e$)

$$\begin{aligned} \mathbf{v}_d &= \frac{e^{-\Phi_g/a_T^2} \nabla q}{n_i \mu_i \nu_i} \\ &= \frac{e^{-\Phi_g/a_T^2}}{n_i \mu_i \nu_i} \left(\frac{dq}{d\Phi_B} \right) \nabla \Phi_B. \end{aligned} \quad (10.11)$$

Referring to Figure 10.1 we can write for the normal vector

$$\begin{aligned} \mathbf{n} &= \frac{\nabla \Phi_B}{|\nabla \Phi_B|} \\ &= \frac{1}{|\nabla \Phi_B|} \left(\frac{\partial \Phi_B}{\partial \varpi} \mathbf{e}_\varpi + \frac{\partial \Phi_B}{\partial z} \mathbf{e}_z \right) \\ &= \frac{1}{|\nabla \Phi_B|} \left(\frac{\partial \Phi_B}{\partial \varpi} \right) \left[\mathbf{e}_\varpi + \left(\frac{\partial \varpi}{\partial z} \right)_{\Phi_B} \mathbf{e}_z \right] \\ &= \frac{\left[\mathbf{e}_\varpi + \left(\frac{\partial \varpi}{\partial z} \right)_{\Phi_B} \mathbf{e}_z \right]}{\left[1 + \left(\frac{\partial \varpi}{\partial z} \right)_{\Phi_B}^2 \right]^{1/2}}. \end{aligned} \quad (10.12)$$

Insertion of equations (10.11) and (10.12) into equation (10.9) we get

$$\left(\frac{\partial M}{\partial t} \right)_{\Phi_B} = \frac{4\pi}{n_i \mu_i \nu_i} \frac{dq}{d\Phi_B} \int_0^{z_{cl}(\Phi_B)} \varpi \frac{\partial \Phi_B}{\partial \varpi} \left[1 + \left(\frac{\partial \varpi}{\partial z} \right)_{\Phi_B}^2 \right]^{1/2} e^{-\Phi_g/a_T^2} dz, \quad (10.13)$$

where we have used

$$\nabla \Phi_B = \frac{\partial \Phi_B}{\partial \varpi} \left(\mathbf{e}_\varpi + \frac{\partial \varpi}{\partial z} \mathbf{e}_z \right). \quad (10.14)$$

This integral must then be continually evaluated to estimate the mass $M(\Phi_B)$ contained in a given magnetic flux tube, include it in equation (9.51), and use equations (9.48) and (9.49) to solve for cloud models that include ambipolar diffusion. Results for such a simulation are shown in Figure 10.2. The initial configuration was that of a cylinder of half-eight and radius of 0.75 pc, threaded by a poloidal magnetic field of 30 μG in strength, and of 300 cm^{-3} density. The initial mass to flux ratio is subcritical.

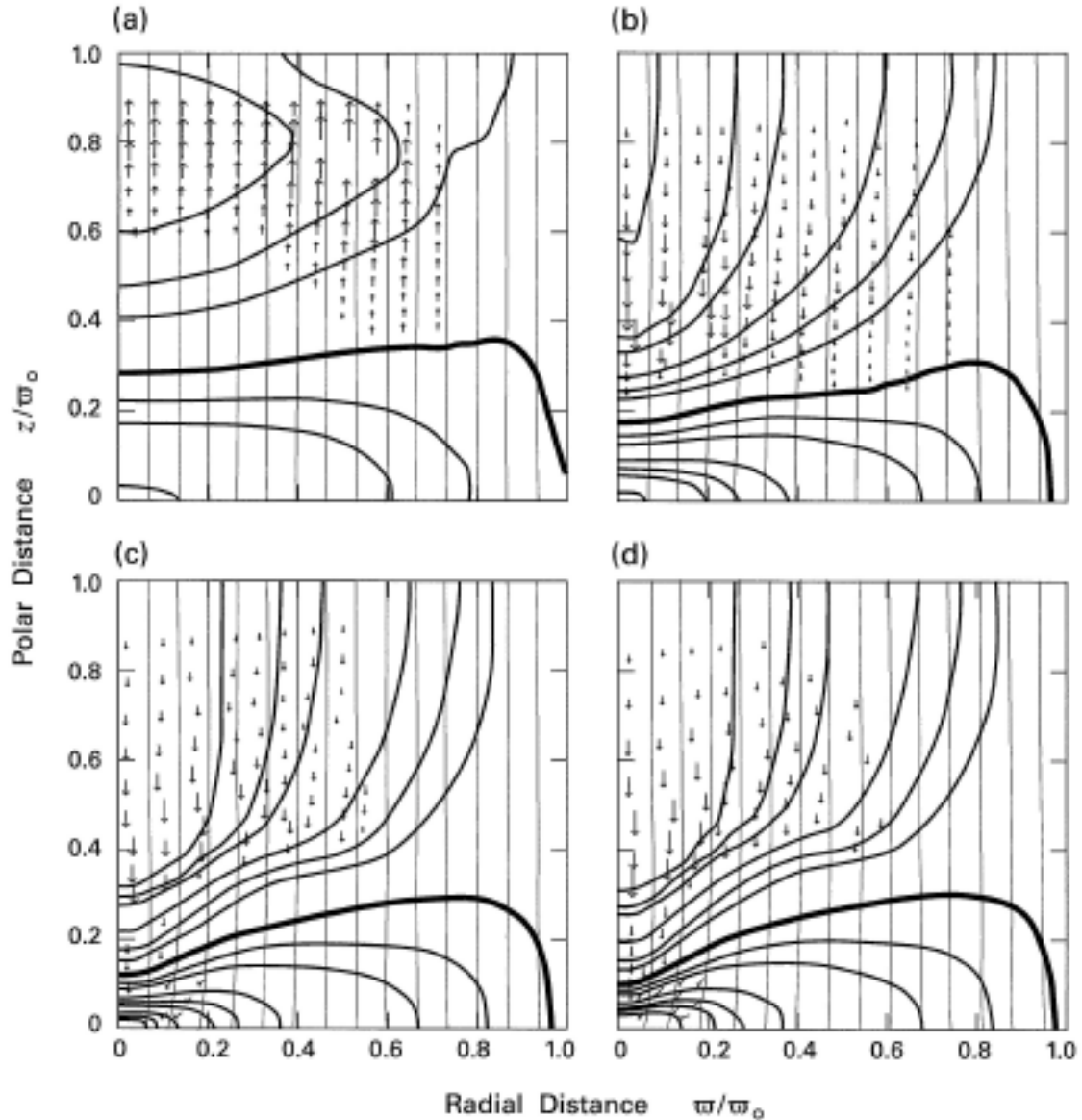


Figure 10.2 – Numerical simulation of a contracting, magnetized cloud, with inclusion of ambipolar diffusion, at times (a) 1.02×10^7 yr, (b) 1.51×10^7 yr, (c) 1.6×10^7 yr, and (d) 1.61×10^7 yr. Light and heavy curves are for magnetic field lines and density contours, respectively. The thick curve corresponds to a density of 300 cm^{-3} , and arrows are the relative fluid velocity.

The change in central density as a function of time is also shown in Figure 10.3. Note that once a high enough central density has been reached at $t > 1.5 \times 10^7$ yr (panel (c) in Figure 10.2), then ambipolar diffusion sets in (i.e., the mass to flux ratio becomes supercritical) and the central core of the cloud can also proceed across the magnetic field lines. Bending in the field lines is also evident. We note, however, that the basic shape of the resulting cloud has not been qualitatively altered, which also means that *this more sophisticated model fails to match observations as well*.

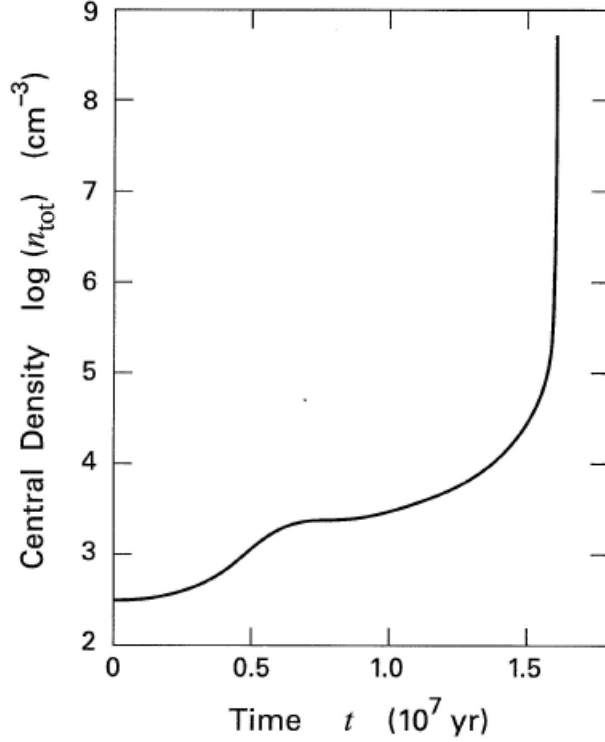


Figure 10.3 – Rise of the central density of the contracting cloud simulated in Figure 10.2.

10.1.2 Damping of Alfvén Waves

We have already determined that Alfvén waves can provide significant support on sufficiently large scales in molecular cloud. We now want to make certain of this by verifying that only waves of length much larger than that of a core can propagate. To do so, we go back to our previous analysis of Chapter 9 (see the Appendix) and consider the dispersion relation calculated when keeping the neutral and plasma fluids separated. Therefore, neglecting gravity our set of equations to solve for is

$$\begin{aligned}
 \frac{\partial(\delta\rho)}{\partial t} + \rho_0 \nabla \cdot \delta\mathbf{u} &= 0 \\
 \rho_0 \frac{\partial(\delta\mathbf{u})}{\partial t} + a_T^2 \nabla(\delta\rho) - \mu_i n_i \nu_i (\delta\mathbf{u}_i - \delta\mathbf{u}) &= 0 \\
 \frac{1}{4\pi} [\nabla \times (\delta\mathbf{B})] \times \mathbf{B}_0 - \mu_i n_i \nu_i (\delta\mathbf{u}_i - \delta\mathbf{u}) &= 0 \\
 \frac{\partial(\delta\mathbf{B})}{\partial t} - \nabla \times (\delta\mathbf{u}_i \times \mathbf{B}_0) &= 0,
 \end{aligned} \tag{10.15}$$

where, as can be guessed, we have already set things up for our usual linear perturbation analysis. We thus proceed with a consideration of a single Fourier component and transform equations (10.15) to

$$\begin{aligned}
& -i\omega\delta\rho + i\rho_0\mathbf{k} \cdot \delta\mathbf{u} = 0 \\
& -i\omega\rho_0\delta\mathbf{u} + a_7^2\delta\rho\mathbf{k} - \mu_i n_i v_i (\delta\mathbf{u}_i - \delta\mathbf{u}) = 0 \\
& \frac{i}{4\pi} [(\mathbf{k} \cdot \mathbf{B}_0)\delta\mathbf{B} - (\mathbf{k} \cdot \delta\mathbf{B})\mathbf{B}_0] - \mu_i n_i v_i (\delta\mathbf{u}_i - \delta\mathbf{u}) = 0 \\
& -i\omega\delta\mathbf{B} - i[(\mathbf{k} \cdot \mathbf{B}_0)\delta\mathbf{u}_i - (\mathbf{k} \cdot \delta\mathbf{u}_i)\mathbf{B}_0] = 0.
\end{aligned} \tag{10.16}$$

Since we know from equations (9.80) that for Alfvén waves the first of these equations gives $\delta\rho = \mathbf{k} \cdot \delta\mathbf{u}_i = 0$ and the $\mathbf{k} \cdot \delta\mathbf{B} = 0$, then the remaining equations reduce to

$$\begin{aligned}
& -i\omega\rho_0\delta\mathbf{u} - \mu_i n_i v_i (\delta\mathbf{u}_i - \delta\mathbf{u}) = 0 \\
& \frac{i}{4\pi} (\mathbf{k} \cdot \mathbf{B}_0)\delta\mathbf{B} - \mu_i n_i v_i (\delta\mathbf{u}_i - \delta\mathbf{u}) = 0 \\
& \omega\delta\mathbf{B} + (\mathbf{k} \cdot \mathbf{B}_0)\delta\mathbf{u}_i = 0.
\end{aligned} \tag{10.17}$$

We next insert the first of these equations into the second to get

$$\frac{i}{4\pi} (\mathbf{k} \cdot \mathbf{B}_0)\delta\mathbf{B} - \mu_i n_i v_i \delta\mathbf{u}_i \left(\frac{i\omega\rho_0}{i\omega\rho_0 - \mu_i n_i v_i} \right) = 0, \tag{10.18}$$

or

$$\begin{aligned}
\delta\mathbf{u}_i &= - \left(1 - \frac{i\omega n}{n_i v_i} \right) \frac{(\mathbf{k} \cdot \mathbf{B}_0)\delta\mathbf{B}}{4\pi\omega\rho_0} \\
&= - \left(1 - \frac{i\omega}{\chi_i v_i} \right) \frac{(\mathbf{k} \cdot \mathbf{B}_0)\delta\mathbf{B}}{4\pi\omega\rho_0},
\end{aligned} \tag{10.19}$$

where we used $n \simeq \rho_0/\mu_i$ and $\chi_i \equiv n_i/n$ for the ionization fraction. We finally substitute the last of equations (10.17) for $\delta\mathbf{B}$ to get

$$\left[1 - \left(1 - \frac{i\omega}{\chi_i v_i} \right) \frac{(\mathbf{k} \cdot \mathbf{B}_0)^2}{4\pi\omega^2\rho_0} \right] \delta\mathbf{u}_i = 0, \tag{10.20}$$

or if we restrict ourselves to the simpler case where \mathbf{k} and \mathbf{B}_0 are parallel

$$\omega^2 + \frac{iv_A^2 k^2}{\chi_i v_i} \omega - v_A^2 k^2 = 0, \tag{10.21}$$

with $v_A = B_0/\sqrt{4\pi\rho_0}$ the Alfvén speed. This is a simple quadratic equation in ω that is readily solved to yield

$$\omega = \frac{1}{2} \left[-\frac{iv_A^2 k^2}{\chi_i v_i} \pm v_A k \sqrt{4 - \left(\frac{v_A k}{\chi_i v_i} \right)^2} \right]. \quad (10.22)$$

We therefore see that the first term on the right hand side of equation (10.22) will bring an exponential decay with time in the amplitude of the Alfvén wave resulting from the perturbation. The time necessary to effect this damping is (in term of the wave's power)

$$\begin{aligned} \tau_{\text{damp}} &\approx \frac{\chi_i v_i}{v_A^2 k^2} \\ &= 1 \times 10^4 \left(\frac{\lambda}{0.06 \text{ pc}} \right)^2 \left(\frac{B}{10 \mu\text{G}} \right)^{-2} \left(\frac{n_{\text{H}_2}}{10^3 \text{ cm}^{-3}} \right)^{3/2} \text{ yr}, \end{aligned} \quad (10.23)$$

where equations (8.57) and (10.4) were used. The Alfvén wave with the shortest wavelength that can propagate is determined from equation (10.22) when

$$\frac{v_A k}{\chi_i v_i} < 2, \quad (10.24)$$

or

$$\begin{aligned} \lambda_{\text{min}} &= \frac{\pi v_A}{\chi_i v_i} \\ &= 0.06 \left(\frac{B}{10 \mu\text{G}} \right) \left(\frac{n_{\text{H}_2}}{10^3 \text{ cm}^{-3}} \right)^{-1} \text{ pc}. \end{aligned} \quad (10.25)$$

We see from equations (10.23) and (10.25) that a wave with $\lambda \approx 30\lambda_{\text{min}}$ will survive for the typical lifetime of a cloud (i.e., 10^7 yr).

10.2 Inside-out Collapse

We now study the collapse of a dense core in the region that is located between the region where there is significant magnetic support (i.e., in the larger scale where $10^{17} \text{ cm} \lesssim L \lesssim 10^{18} \text{ cm}$) and the region close to the nascent protostar where magnetic field support has been removed through ambipolar diffusion ($10^{11} \text{ cm} \lesssim L \lesssim 10^{14} \text{ cm}$). To carry this program we concentrate once again on a spherical isothermal sphere, but one that is slightly more massive than the Bonner-Ebert sphere studied in Chapter 9 (i.e., slightly on the right of the maximum of the curve shown in Figure 9.2). We first write the equations needed to solve the problem (numerically). The mass contained within a radius r is

$$M_r = \int_0^r 4\pi r'^2 \rho dr'. \quad (10.26)$$

It follows that

$$\begin{aligned} \frac{\partial M_r}{\partial r} &= 4\pi r^2 \rho \\ \frac{\partial M_r}{\partial t} &= 4\pi \int_0^r r'^2 \frac{\partial \rho}{\partial t} dr' \\ &= -4\pi \int_0^r r'^2 \left[\frac{1}{r'^2} \frac{\partial (r'^2 \rho u)}{\partial r'} \right] dr' \\ &= -4\pi \int_0^r d(r'^2 \rho u) \\ &= -4\pi r^2 \rho u, \end{aligned} \quad (10.27)$$

where the equation of continuity was used

$$\frac{\partial \rho}{\partial t} = -\frac{1}{r^2} \frac{\partial (r^2 \rho u)}{\partial r}. \quad (10.28)$$

Furthermore, the equation of motion (including the non-linear term) is

$$\frac{\partial u}{\partial t} + u \frac{\partial u}{\partial r} = -\frac{a_T^2}{\rho} \frac{\partial \rho}{\partial r} - \frac{GM_r}{r^2}. \quad (10.29)$$

With these equations (i.e., (10.27) to (10.29)) boundary conditions of the *constant pressure* or *constant volume* types are usually used, and the problem is solved numerically. The results from one such simulation is shown in Figure 10.4 for the infall velocity (normalized to the sound speed) as a function of the dimensionless radius. It is thus found that the sphere is collapsing in an inside-out manner, the so-called **inside-out collapse**. This main feature is highly insensitive of the boundary (initial) conditions. It is found that starting at the boundary of the cloud, the velocity grows until every mass shell is accelerating inward. The evolution of the central part of the cloud is very difficult to follow numerically, however, and one usually simplifies matter by numerically collecting the infalling matter into a **sink-cell**, while keeping track of the amount of mass falling within it. The protostar is assumed to accrete this mass.

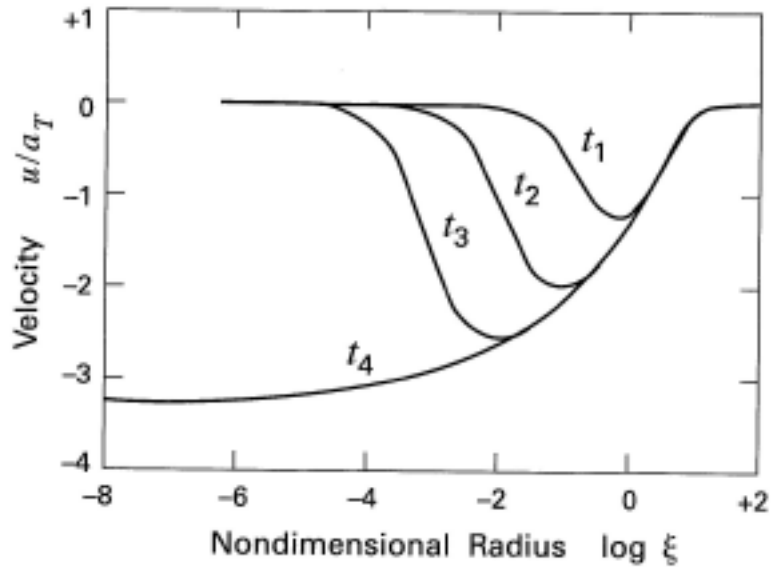


Figure 10.4 – Velocity profiles in a collapsing, isothermal sphere as a function of the dimensionless radius ξ (see equation (9.10)). The four times are measured in units of the free-fall time, t_{ff} (see equation (3.21)), with $t_1 = -0.0509$, $t_2 = -0.0026$, $t_3 = -0.0001$, and $t_4 = 0$, the latter being the time of protostar formation. The free-fall time is that associated to the initial central density.

10.2.1 The Mass Accretion Rate

The concept of inside-out collapse is perhaps easier to grasp by monitoring the **mass accretion rate**, \dot{M} , into the sink-cell. This parameter determines the growth rate of the protostar and is mathematically defined as

$$\begin{aligned} \dot{M} &\equiv \lim_{r \rightarrow 0} \frac{\partial M}{\partial t} \\ &= \lim_{r \rightarrow 0} (-4\pi r^2 \rho u), \end{aligned} \quad (10.30)$$

from the last of equations (10.27). The results from two simulations that started with different initial density contrasts are shown in Figure 10.5. It is seen that the accretion rate is initially relatively high before leveling off to a value of

$$\dot{M} = m_0 \frac{a_T^3}{G}, \quad (10.31)$$

where m_0 is on the order of unity. We can interpret this equation as follows. When a protostar is formed then the gas nearby it is in free-fall, since gravity will be dominant over thermal pressure. We can then write for the free-fall velocity

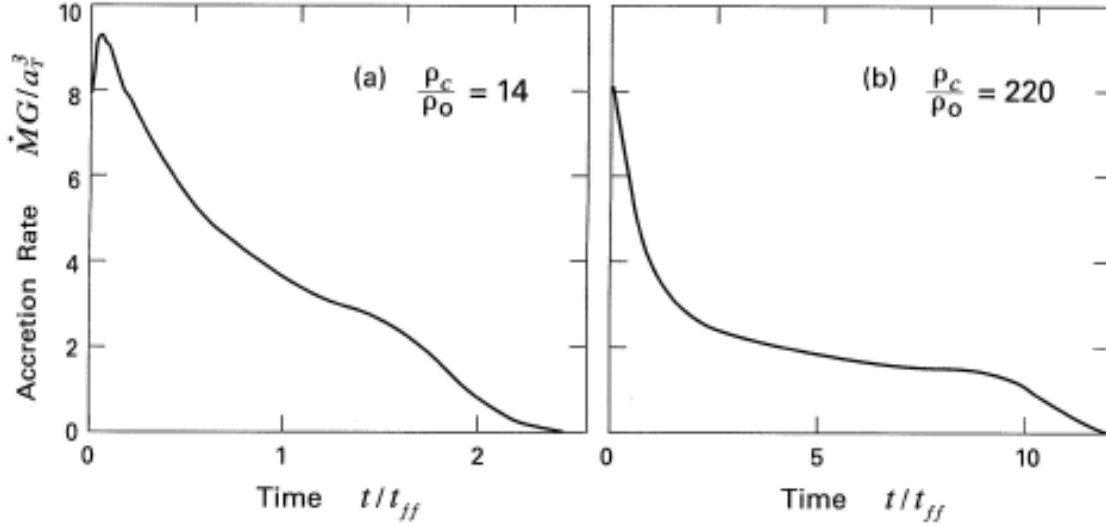


Figure 10.5 – Time evolution of the mass accretion rate for two different initial density contrasts.

$$V_{ff} \equiv \left(\frac{2GM_*}{r} \right)^{1/2}, \quad (10.32)$$

where $M_* \approx \dot{M}t$ is the time-dependent mass of protostar. Of course, the gravitational pull of the protostar weakens with the radius and stops when

$$a_T^2 \left| \frac{\partial \rho}{\partial r} \right| \approx \rho \left| \frac{\partial}{\partial r} \left(\frac{GM_*}{r} \right) \right|, \quad (10.33)$$

or

$$a_T^2 \frac{\rho}{r} \approx \rho \frac{GM_*}{r^2} \quad (10.34)$$

from hydrostatic equilibrium considerations, which implies that

$$a_T \approx V_{ff}. \quad (10.35)$$

The radius, R_{ff} , at which this occur is found to be such that

$$\begin{aligned} \dot{M} &\approx \frac{a_T^2}{G} \frac{R_{ff}}{t} \\ &\approx \frac{a_T^2 \dot{R}_{ff}}{G}, \end{aligned} \quad (10.36)$$

with $\dot{R}_{\text{ff}} \approx R_{\text{ff}}/t$. We then find that $\dot{R}_{\text{ff}} > 0$ as long as $\dot{M} > 0$, and the region of free-fall spreads with time as long there is some mass left to be accreted by the protostar. That is, a given shell of the sphere cannot collapse until the shell below it has already free-fallen. This is the essence of the inside-out collapse. This propagation happens at the speed of sounds, as can be guessed from Figure 10.5. Setting $\dot{R}_{\text{ff}} = a_T$ in equation (10.36) we approximately recover equation (10.31), which can be favorably transformed to

$$\dot{M} \approx 2 \times 10^{-6} M_{\odot} \left(\frac{T}{10 \text{ K}} \right)^{3/2} \text{ yr}^{-1}. \quad (10.37)$$

This relation implies that a $1 M_{\odot}$ protostar accretes its mass over approximately $5 \times 10^5 \text{ yr}$, which is very small compared to its contraction time ($\sim 10^7 \text{ yr}$).

The inside-out collapse can also be investigated as follows. For the shell that is positioned just beyond the free-falling region, where matter free-falls at an approximately constant rate, we can write the equation of continuity as

$$\begin{aligned} \frac{\partial \rho}{\partial t} &= -\frac{1}{r^2} \frac{\partial(r^2 \rho u)}{\partial r} \\ &= 0, \end{aligned} \quad (10.38)$$

which implies from equation (10.30) that

$$\begin{aligned} \dot{M} &= -4\pi r^2 \rho u \\ &= \text{constant}. \end{aligned} \quad (10.39)$$

Setting $u = -V_{\text{ff}}$ from equation (10.32) we find that

$$\rho = \frac{\dot{M} r^{-3/2}}{4\pi \sqrt{2GM_*}}, \quad (10.40)$$

which implies that the density of that shell decreases with time. The picture that comes out of equation (10.40) is shown schematically in Figure 10.6.

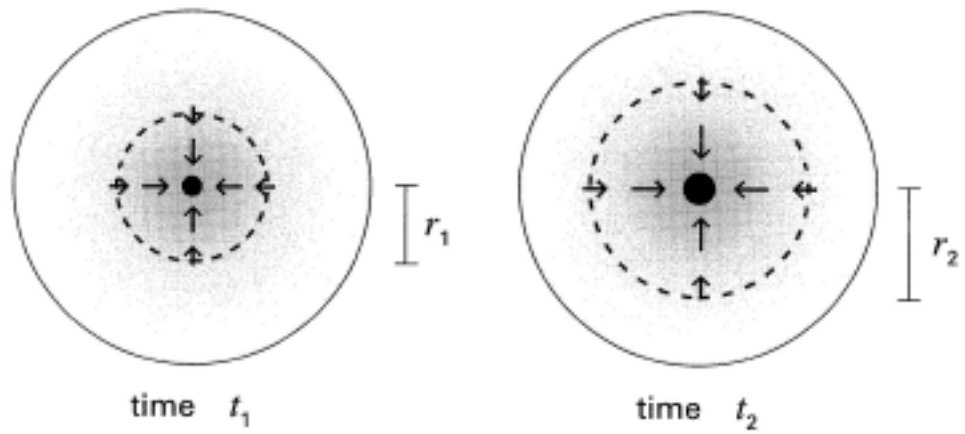
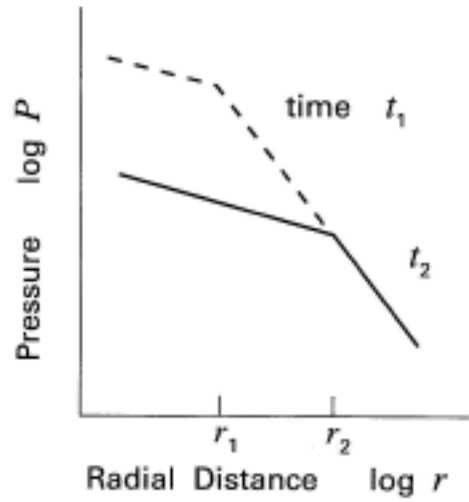


Figure 10.6 – The inside-out collapse and the pressure profile at two different times.